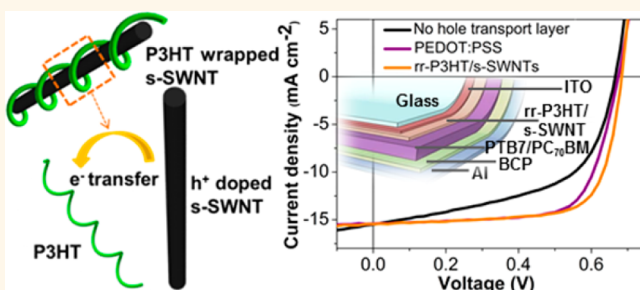


Hybrid Carbon Nanotube Networks as Efficient Hole Extraction Layers for Organic Photovoltaics

G. Dinesha M. R. Dabera,^{†,§} K. D. G. Imalka Jayawardena,^{†,§} M. R. Ranga Prabhath,[†] Iskandar Yahya,[†] Y. Yuan Tan,[†] N. Aamina Nismy,[†] Hidetsugu Shiozawa,[‡] Markus Sauer,[‡] G. Ruiz-Soria,[‡] Paola Ayala,[‡] Vlad Stolojan,[†] A. A. Damitha T. Adikaari,^{†,‡} Peter D. Jarowski,[†] Thomas Pichler,[‡] and S. Ravi P. Silva^{†,*}

[†]Advanced Technology Institute, University of Surrey, Guildford, Surrey, GU2 7XH, United Kingdom and [‡]Elektronische Materialeigenschaften, Fakultät für Physik, Universität Wien, Strudlhofgasse, 4, 1090, Wien, Austria. [§]These authors contributed equally to this work. [†]Present address: Department of Energy & Climate Change, 3 Whitehall Place, London, SW1A 2AW, United Kingdom.

ABSTRACT Transparent, highly percolated networks of regioregular poly(3-hexylthiophene) (rr-P3HT)-wrapped semiconducting single-walled carbon nanotubes (s-SWNTs) are deposited, and the charge transfer processes of these nanohybrids are studied using spectroscopic and electrical measurements. The data disclose hole doping of s-SWNTs by the polymer, challenging the prevalent electron-doping hypothesis. Through controlled fabrication, high-to low-density nanohybrid networks are achieved, with low-density hybrid carbon nanotube networks tested as hole transport layers (HTLs) for bulk heterojunction (BHJ) organic photovoltaics (OPVs). OPVs incorporating these rr-P3HT/s-SWNT networks as the HTL demonstrate the best large area (70 mm²) carbon nanotube incorporated organic solar cells to date with a power conversion efficiency of 7.6%. This signifies the strong capability of nanohybrids as an efficient hole extraction layer, and we believe that dense nanohybrid networks have the potential to replace expensive and material scarce inorganic transparent electrodes in large area electronics toward the realization of low-cost flexible electronics.



KEYWORDS: carbon nanotubes · organic photovoltaics · rr-P3HT/s-SWNT · nanohybrids · hole transport layer

Single-walled carbon nanotubes (SWNTs) with their unique electronic transport properties continue to contribute to rapid advances in the fields of flexible electronics,¹ photovoltaics,² thin-film transistors (TFTs),³ and biosensors.⁴ Traditionally, as-produced carbon nanotubes are known to form bundles, which prevents the unique properties of individual carbon nanotubes being realized. As a result, techniques such as covalent⁵ and noncovalent functionalization⁶ have been utilized for isolating individual nanotubes. Recently, self-assembly of polymers into a supramolecular shell wrapping s-SWNTs has been gaining popularity as a route toward incorporation of nanotubes into organic optoelectronic devices^{7,8} as well as for the fabrication of wafer-scale thin-film TFTs.³

Despite the widespread use of polymer-wrapped nanotubes, the nature of the charge transport within the nanotube (*i.e.*, its electron or hole conduction) has remained a

matter of debate. While spectroscopic evidence has indicated an electron transfer to s-SWNTs from rr-P3HT,^{7,9,10} charge transport analysis has hinted of a hole transfer process.¹¹

In the field of organic photovoltaics (OPVs), carbon nanotubes (CNTs) have been identified as promising candidates for excitonic antennas and concentrators,¹² broad-band energy harvesters,¹³ additional exciton dissociation sites in triple heterojunctions,¹⁴ and as high mobility charge extraction paths.¹⁵ Over the past few years, much effort has been expanded on producing a material system that can act as an efficient hole extraction layer for OPVs as a substitute for poly(3,4-ethylenedioxythiophene):poly(styrenesulfonate) (PEDOT:PSS), the most common hole extraction material used.^{15–17} The hygroscopicity and acidity of PEDOT:PSS cause degradation of the active layer and the indium tin oxide (ITO) electrode resulting in a decreased lifetime of the solar cell.¹⁶

* Address correspondence to s.silva@surrey.ac.uk.

Received for review October 10, 2012 and accepted December 12, 2012.

Published online December 12, 2012
10.1021/nn304705t

© 2012 American Chemical Society

Among the potential solution-processable candidates, CNTs have attracted much attention with recent reports indicating a power conversion efficiency (PCE) of 4.9% under AM 1.5G 1.3 sun illumination for OPVs incorporating CNTs as the hole extraction layer.¹⁸

In this study, strong evidence for preferential hole transport in solution-processable large area networks of polymer-wrapped s-SWNT networks is presented, indicating the role of such nanohybrids as hole extraction layers. In order to investigate the nanohybrids performing in the capacity of hole transport layers (HTLs) in OPVs, devices were fabricated with rr-P3HT/s-SWNTs as the HTL with rr-P3HT/PC₇₀BM ([6,6]-phenyl-C71-butrylic acid methyl ester) as the active photo-absorption layer. These investigations were further expanded for active layers based on the low band gap donor polymer PTB7 (poly[[4,8-bis[(2-ethylhexyl)oxy]benzo[1,2-b:4,5-b']dithiophene-2,6-diyl][3-fluoro-2-(2-ethylhexyl)carbonyl]thieno[3,4-b]thiophenediyl]])/PC₇₀BM system.

Under an AM 1.5G 1 sun illumination, the PTB7/PC₇₀BM fabricated devices displayed a PCE of 7.6%, which is not only the best achieved for OPVs without a traditional hole transport layer but also the best reported for organic solar cells utilizing carbon nanotubes as an active element to date.^{7,18}

RESULTS AND DISCUSSION

Nanoscale Ordering of the Polymer on the Nanotubes. To obtain a good dispersion, s-SWNTs were supramolecularly functionalized using rr-P3HT. Preparation of the rr-P3HT/s-SWNT nanohybrids was achieved through sonication of high-purity (90%) s-SWNTs (0.50 mg) with rr-P3HT (0.60 mg) in 1.00 mL of chlorobenzene. The removal of excess rr-P3HT was achieved through a solvent extraction technique reported by Nish *et al.*¹⁹ using toluene as the extraction solvent with the prepared nanohybrids dispersed in 2.00 mL of 1,2-dichlorobenzene. The final weight ratio between rr-P3HT and s-SWNTs was \sim 1:3. Semiconducting nanotube-enriched material in this study helped optimize device performance, which is known to be compromised due to the presence of metallic nanotubes.²⁰

Spin-coating these nanohybrid solutions onto ITO-coated glass substrates at 500 and 1500 rpm is observed to lead to a network of nanohybrids as imaged using atomic force micrographs (AFM) (Figure 1B,C) over an area of $5\text{ }\mu\text{m} \times 5\text{ }\mu\text{m}$. In terms of the geometry of rr-P3HT in the presence of SWNTs, previous reports on nanohybrids prepared using techniques similar to that described in this work have indicated experimentally (through scanning probe microscopic techniques), as well as computationally, a natural tendency for the rr-P3HT to wrap around SWNTs due to π - π -type supermolecular interactions.^{10,21-24} To ascertain this fact further and to obtain a better understanding of the noncovalent functionalization process, optical

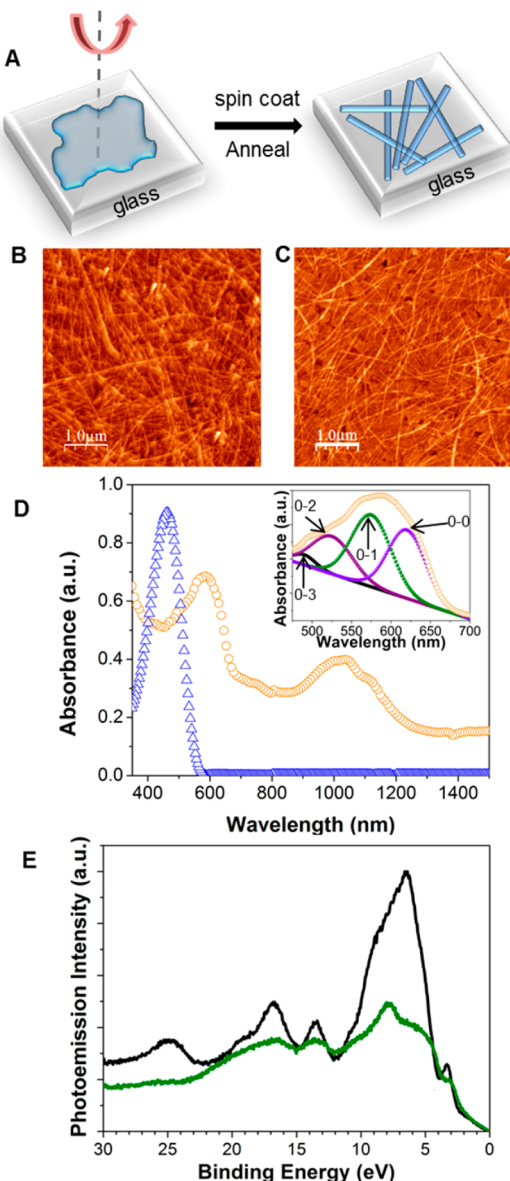


Figure 1. AFM images of rr-P3HT/s-SWNTs spin-coated on ITO/glass, absorption spectra, and XPS analysis of nanohybrids. (A) Schematic representation of the spin-casting process of nanohybrids from solution followed by thermal annealing giving rise to a network of nanohybrids. (B) Highly dense percolative network of nanohybrids ($5\text{ }\mu\text{m} \times 5\text{ }\mu\text{m}$) spin-coated from a $\sim 0.5\text{ mg mL}^{-1}$ solution at a spin speed of 500 rpm on ITO/glass, and (C) image of a nanohybrid film spin-coated at 1500 rpm from the same solution. The ITO surface is visible at this stage. (D) UV-vis-NIR absorption spectra of rr-P3HT/s-SWNT (orange circles) and pristine rr-P3HT (blue triangles) dispersions in 1,2-dichlorobenzene with a red shift in the 460 nm peak of rr-P3HT to 590 nm in the rr-P3HT/s-SWNTs, indicating the increased crystallinity of rr-P3HT in nanohybrids. The inset shows an expansion of the rr-P3HT/s-SWNT absorption spectrum in the range of 475–700 nm. The fitted peaks are assigned to the 0–0, 0–1, 0–2, and 0–3 transitions revealing the better ordered nature of rr-P3HT due to π - π stacking with s-SWNTs. (E) Low-energy XPS valence band spectra of rr-P3HT/s-SWNTs (green line) and s-SWNTs (black line) obtained at a photon energy of 125 eV.

absorption, valence, and core level X-ray spectroscopy (XPS) measurements were carried out on the rr-P3HT/s-SWNT nanohybrid system.

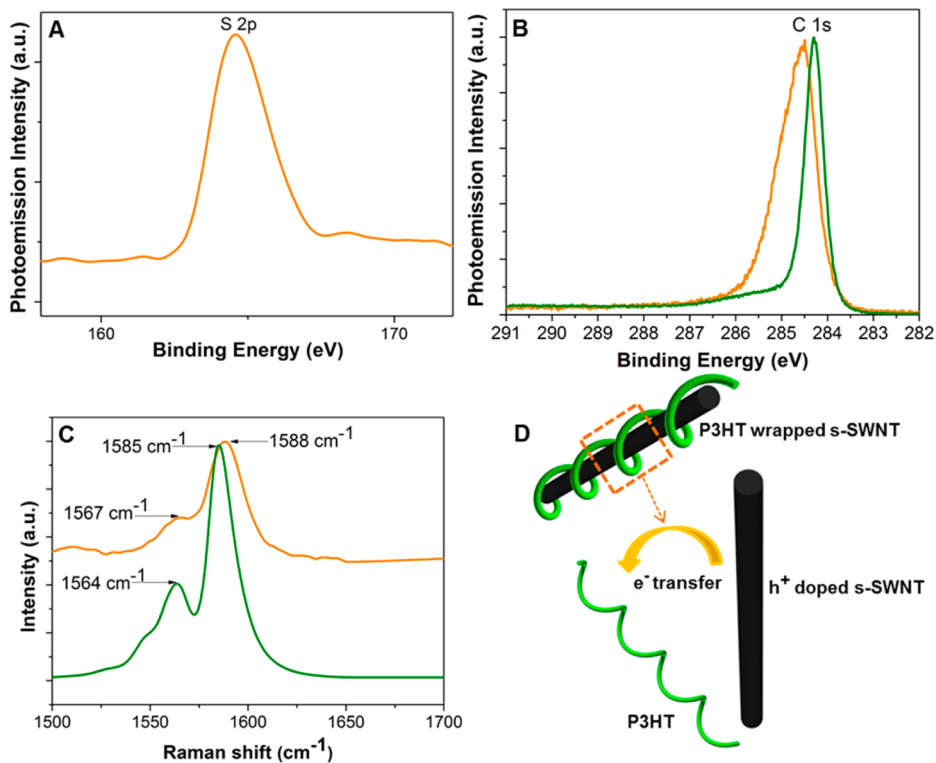


Figure 2. XPS and Raman G-band spectra of s-SWNTs and rr-P3HT/s-SWNTs. (A) Core level XPS S 2p spectrum of rr-P3HT/s-SWNTs (orange line) obtained at a photon energy of 1250 eV. (B) Core level XPS C 1s spectra of rr-P3HT/s-SWNTs (orange line) and s-SWNTs (green line) obtained at a photon energy of 400 eV. (C) Raman G-band spectra indicating an upshift of 3 cm^{-1} in nanohybrids compared to pristine s-SWNTs. (D) Schematic diagram of a P3HT-wrapped s-SWNT and the charge transfer process from the s-SWNT to P3HT creating hole-doped carbon nanotubes.

A representative UV-vis absorbance spectrum for rr-P3HT/s-SWNT nanohybrids in 1,2-dichlorobenzene is shown in Figure 1D. The analysis of the spectroscopic evidence for the nanohybrids in comparison to free rr-P3HT indicates a large red shift of the absorption edge of rr-P3HT (from ~ 460 to ~ 590 nm) due to $\pi-\pi^*$ transitions^{19,25} upon the formation of the nanohybrids. The red shift coupled with the disappearance of the 460 nm absorption edge is due to the increased long-range order of rr-P3HT chains as a result of $\pi-\pi$ stacking with s-SWNTs in the polymer wrapping of carbon nanotubes.¹⁹ Furthermore, the absorbance spectrum of rr-P3HT/s-SWNTs indicates a structure within the wavelength region of 470–630 nm corresponding to vibronic progressions described by the Franck-Condon principle (Figure 1D, inset).²⁶ The near unity value for the 0–0 to 0–1 intensity ratio combined with the low intensity for the 0–2 and 0–3 (relative to 0–1 peak)¹⁹ supports the ordering of rr-P3HT radial to the nanotubes, indicating nanoscale ordering of rr-P3HT in an individual nanohybrid.

The nature of rr-P3HT surrounding the s-SWNTs was further examined using valence level X-ray photoelectron spectroscopy (XPS). The valence band spectra of s-SWNT and rr-P3HT/s-SWNT shown in Figure 1E display an increase in the delocalized C 2p π signal (~ 4 – 7 eV)²⁷ in rr-P3HT/s-SWNTs than in the pristine s-SWNTs. The result should be an enhanced charge

transport in the nanohybrids compared to pristine s-SWNTs. Furthermore, the lack of any discernible features in the range of 8.2–13.5 eV in the valence band spectrum of the nanohybrid results from a loss/weakening of $\pi-\pi$ interactions between the P3HT chains due to tilting of adjacent polymer chains²⁸ and can be taken as indirect evidence for the polymer wrapping of nanotubes.

Further evidence for the nature of the interaction between rr-P3HT with the nanotubes is observed through the S 2p peak (due to carbon–sulfur bonding in rr-P3HT) at a binding energy (BE) of 164.5 eV²⁹ of the core level X-ray photoelectron spectrum (Figure 2A). The spin-orbit splitting corresponding to the S 2p $^{3/2}$ and S 2p $^{1/2}$ states expected for free rr-P3HT with an intensity ratio of 2:1 is not observed, which is attributed to the high crystallinity of rr-P3HT in the nanohybrids³⁰ and/or interactions between S atoms in rr-P3HT with the s-SWNTs.²⁹ The possibility for higher crystallinity is further supported by the absence of satellite peaks on the high BE side at ~ 290 eV in the C 1s spectrum (Figure 2B), which indicates a lack of fragments with a smaller conjugation length.^{29,31}

Charge Transfer between the Polymer and Nanotubes.

Although the role of nanotubes in OPVs has been actively investigated, there still appears to be no clear consensus as to the nature of the charge transfer interaction between rr-P3HT and SWNTs. While the

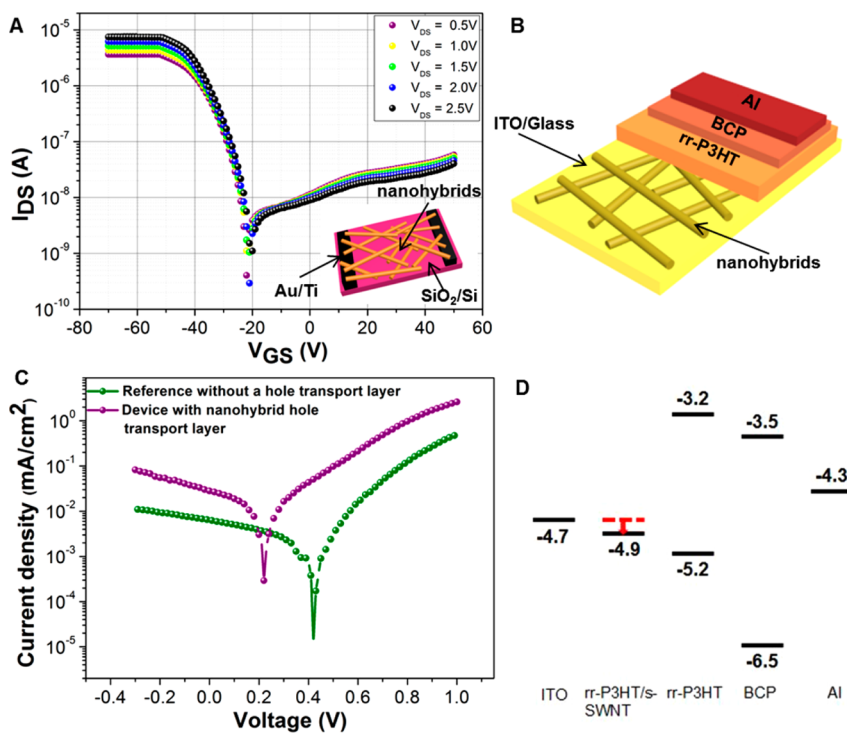


Figure 3. Transfer characteristics and J – V curves of “hole only” devices of nanohybrids. (A) Transfer characteristics of the self-ordered nanohybrids for channel lengths of $10\ \mu\text{m}$ under a V_{DS} range of 0.5 to 2.5 V. A prominent hole transportation is observed under negative gate biasing with a significantly weaker electron transportation under positive biasing, indicating the preferential hole transport behavior of the nanohybrids. Measurements were carried out under a N_2 atmosphere using a 230 nm SiO_2 gate dielectric with a global bottom gate and Au bottom contacts (inset). (B) Schematic of the device architecture used for the nanohybrids incorporated device. (C) Response of the reference P3HT only and nanohybrid incorporated rr-P3HT hole only devices under illumination with AM 1.5G simulated light. (D) Flat band diagram for the nanohybrid incorporated device used, and the down shift of the ionization potential of s-SWNTs due to hole doping by rr-P3HT is indicated by the red arrow. The band alignment favors the transportation of holes to ITO, leading to the observation of fourth quadrant characteristics for the nanohybrid incorporated devices in (D).

commonly held view has been an electron transfer from rr-P3HT.^{9,10} Dissanayake and Zhong¹¹ reported a hole transfer to individual or few nanotubes in the presence of rr-P3HT. Therefore, the charge transfer process between wrapped rr-P3HT and s-SWNTs was examined using core level XPS and Raman spectroscopy.

Analysis of the S 2p and C 1s of the core level XPS spectra of the nanohybrids (Figure 2A,B) indicates a downshift of the BE for the former (~ 164.5 eV in the nanohybrid compared to 164.75 eV²⁹ in rr-P3HT) and an upshift for the latter (~ 284.5 eV in the nanohybrid compared to 284.3 eV in s-SWNT). An up (down) shift is attributed to a hole (electron) transfer to the s-SWNT (rr-P3HT).³² This cannot be due to any form of disordering effect caused by blending of rr-P3HT with s-SWNTs as a highly crystalline structure is imparted on the rr-P3HT by s-SWNTs as observed in the absorption and valence level XPS spectra discussed above (and given in Figure 1E). The charge transfer process between the s-SWNTs and the surrounding rr-P3HT was further analyzed by Raman spectroscopy. A small red shift (by $3\ \text{cm}^{-1}$) of the Raman G-band in nanohybrids compared to pure s-SWNTs (Figure 2C) is observed which could occur as a result of hole doping of nanotubes.³³ It is important to note that the hole doping effect due

to exposure to oxygen in the atmosphere can be ruled out as both s-SWNTs and nanohybrid films were prepared and stored under identical conditions. However, as the observed Raman shift is insufficiently robust, field effect transistor (FET) measurements were carried out on the thin films of nanohybrids, where deposition of the film on electrodes and device measurements were all carried out in a N_2 glovebox. The use of a N_2 atmosphere mitigates any unintended hole doping of the nanotubes due to O_2 exposure. Therefore, the observed characteristics are considered to be due to charge transfer processes occurring as a result of the polymer wrapping of the nanotubes.

The transfer characteristics of the nanotubes at a channel length of $10\ \mu\text{m}$ is shown in Figure 3A. Nonlinear I – V characteristics have been observed under $V_g = 0$ V, indicating the formation of a Schottky contact to the nanohybrids. Traditionally, due to its high HOMO level of -5.2 eV, rr-P3HT has been reported to form an Ohmic contact when spin-coated onto Au (work function = -5.1 eV) electrodes,³⁴ while Au is known to form a Schottky contact to carbon nanotubes.³⁵ The observation of nonlinear characteristics therefore indicates that the polymer sheath wrapping the s-SWNT is sufficiently thin to act as a

tunnel barrier allowing for charge transport through the nanotubes. However, the formation of a Schottky contact to nanotubes is considered to be detrimental to device performance by affecting the charge injection and hence the ballistic transport properties,³⁶ as well as leading to ambipolar transport characteristics. This is due to the tunneling of electrons from the contacts to the nanotubes under positive gate voltages,³⁵ especially when measured in vacuum.³⁷

As expected for Schottky barrier s-SWNT transistors, the transfer characteristics indicate a suppressed ambipolar charge transport with an electron transport that is 2–3 orders of magnitude lower in comparison to that of hole transport in the device. Despite this, the weak ambipolar nature leads to relatively low I_{on}/I_{off} ratios of $\sim 10^3$ for negative gate voltages. It is noted that similar observations for preferential hole transport have been made for carbon nanotube FETs measured in air, where hole doping due to exposure to O₂ suppresses the n-type behavior (and hence the ambipolar nature) of the device.³⁷ As the transport measurements have been carried out in N₂ environment, the observed preferential hole transport in the nano-hybrids is attributed to the hole doping of the s-SWNTs due to charge transfer interactions between rr-P3HT and the nanotubes. The measured lateral in-plane transport values for the nano-hybrid structures are observed to be comparable to those reported in the self-organized nanotube networks in SiO₂ by Bao *et al.*³⁸

Nanohybrids as a Hole Extraction Layer in OPVs. The potential of these hole-doped s-SWNTs as hole extraction centers as well as its effect on the dissociation of excitons photogenerated in rr-P3HT was studied using the device architecture depicted in Figure 3B. “Bilayer” heterojunction photovoltaic cells were fabricated by spin-coating the nano-hybrids onto an ITO-coated glass followed by spin-coating a layer of rr-P3HT with the photo characteristics being investigated under exposure to 100 mW cm⁻² AM 1.5G simulated light. The hole collection was carried out on the ITO electrode, while the devices behave as “hole only” structures due to the low exciton diffusion length (of ~ 10 nm¹¹) and a low electron mobility of $\sim 10^{-4}$ cm² V⁻¹ s⁻¹ of rr-P3HT.³⁹ Under dark conditions, a forward rectifying behavior is observed while a fourth quadrant operation is noted upon exposure to light of 100 mW cm⁻² (Figure 3C) with an open circuit voltage of ~ 0.2 V. Furthermore, the observed merging of light and dark characteristics at ~ 0.5 V (see Supporting Information) (which indicates the lack of photocurrent generation) indicates the built-in potential of the system to be at this value.¹¹ On the other hand, rr-P3HT-based devices prepared without the nano-hybrid hole transport layer indicate only a weak fourth quadrant behavior and a higher open circuit voltage of ~ 0.4 V under photoillumination.

According to the metal–insulator–metal model which is traditionally used for describing the behavior

of organic semiconductors sandwiched between two metal contacts, the open circuit voltage is governed by the difference in the work function of the contacts used.⁴⁰ However, in the case of organic heterojunctions formed between two ohmic contacts, the open circuit voltage is known to be better described by the alignment of the quasi-Fermi level of the components.⁴¹ Therefore, the observation of a lower open circuit voltage for the nanotube (whose quasi-Fermi level is closer to that of rr-P3HT) incorporated devices, in comparison to the P3HT only devices (open circuit voltage of ~ 0.4 eV due to work functions of ITO and Al, which are 4.7 and 4.3 eV, respectively) indicates that a heterojunction is formed between the nanotubes and the rr-P3HT. Furthermore, this is confirmed by the enhancement in the short circuit current density for the nanotube incorporated devices when compared to the P3HT only devices. This illustrates that the inclusion of the nanotubes leads to an enhancement in the exciton dissociation and photocurrent generation.¹⁴

Although the hole transporting and exciton dissociation capability of these nano-hybrids is in contradiction to the conclusions made in the literature,⁴² we note that these results are in agreement with those reported by Dissanayake and Zhong for few nanotubes (1–6 tubes)¹¹ coated with rr-P3HT. This is the first report on the hole doping effect by rr-P3HT for large area carbon nanotube networks and confirms the use of these nano-hybrid networks as hole transport layers for organic optoelectronic devices.

Having confirmed the hole transporting nature of the nano-hybrids, we proceed to understand the observed photovoltaic device performance given in Figure 3C through energy level alignments in the device architecture employed (Figure 3D). The built-in potential due to the work function difference of rr-P3HT and rr-P3HT/s-SWNT is ~ 0.5 V. Taking the work function of rr-P3HT to be -4.4 eV, the hole transporting nature of the nano-hybrids requires a lower ionization potential at -4.9 eV.^{11,43} However, the inferred value of the ionization potential of nano-hybrids is lower than the ionization potential of pristine SWNTs (-4.7 eV)¹¹ and further confirms the hole doping of carbon nanotubes by rr-P3HT.

For application of these nano-hybrid films for OPVs, 1–3 nm thin films of low nanotube density (0.02 mg mL⁻¹) were prepared by spin-coating nano-hybrids at a speed of 1500 rpm on ITO/glass, and an AFM image of such a film is given in Figure 4B. A low density of nanotubes prevents the short circuiting of carbon nanotube incorporated OPVs which can occur even in the presence of minute quantities of metallic nanotubes.¹⁰ The nano-hybrids on ITO/glass have a transmission of $\sim 89\%$ at a wavelength of 550 nm (Figure 4A), where a 40 nm thick PEDOT:PSS layer used for the reference device fabrication has a transmission of 85% at the same wavelength.

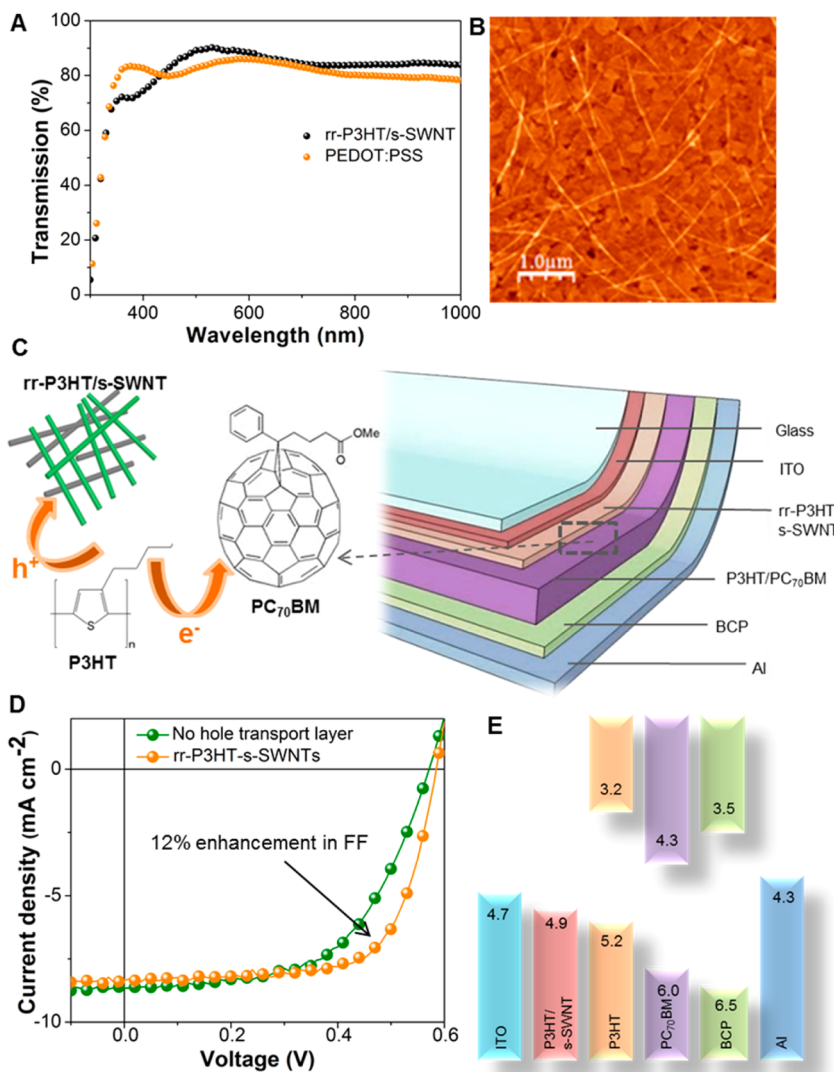


Figure 4. Transmission of nanohybrids, OPV device architecture, and the charge transfer at the interface of the active layer and the hole transport layer along with the corresponding energy level diagram and J – V characteristics of the devices. (A) Transmission spectrum of a typical nanohybrid layer used as the HTL in devices, on ITO/glass, and (B) AFM image of the film displaying the thin but still percolated network of nanohybrids. (C) Schematic representation of the device architecture used to fabricate solution-processed OPV structures employing rr-P3HT/s-SWNT HTLs. The active layer consists of rr-P3HT/PC₇₀BM which is sandwiched between rr-P3HT/s-SWNT hole transport and BCP electron transport layers. ITO acts as the anode, whereas the Al represents the cathode. (D) J – V characteristics of devices A (orange) and B (green) under AM 1.5G illumination with an irradiation intensity of 100 mW cm^{-2} . (E) Suggested band diagram of a device (ITO/(rr-P3HT/s-SWNT)/(rr-P3HT/PC₇₀BM)/BCP/Al) employing rr-P3HT/s-SWNT nanohybrids as an electron-blocking layer. The energy values are in electronvolts.

OPV devices were fabricated by employing nanohybrids as the hole transport layer, and a reference device was also fabricated without a hole transport layer. The active layer of the devices comprised rr-P3HT as the donor and PC₇₀BM as the electron acceptor. The complete device architecture representing different cross sections of the device is depicted in Figure 4C. Evaluation of the effectiveness of the nanohybrid HTL was performed by comparing the device performance of the nanohybrid HTL incorporated device (device type A) with a device without a HTL (device type B). The current density–voltage (J – V) characteristics of a typical device of types A and B under AM 1.5G illumination with an irradiation intensity of 100 mW cm^{-2} are

depicted in Figure 4D, and the device performance characteristics are given in Table 1.

The importance of the nanohybrid HTL is evident by the increase in PCE from 2.8 to 3.4%, through the inclusion of the HTL. The drastic improvement of PCE of device A compared to that of device B is mainly governed by the increased fill factor (FF) of device A by 12% compared to device B. This indicates efficient hole extraction as a result of enhanced interfacial contact between the adjacent layers due to the chemical match between rr-P3HT in the active layer and the HTL, the high mobility of the extracted charges in the HTL, and better ohmic contact between the ITO and HTL.^{40,44} The most important phenomenon for the nanohybrids

TABLE 1. Device Performance Parameters for Devices A and B (A = ITO/(rr-P3HT/PC₇₀BM)/BCP/AI and B = ITO/(rr-P3HT/s-SWNT)/(rr-P3HT/PC₇₀BM)/BCP/AI under AM 1.5G illumination)

device	thickness of the active layer (nm)	V _{oc} (V)	J _{sc} (mA cm ⁻²)	FF (%)	PCE (%)
A = ITO/(rr-P3HT/PC ₇₀ BM)/BCP/AI	210	0.57	8.66	57.03	2.81
B = ITO/(rr-P3HT/s-SWNT)/(rr-P3HT/PC ₇₀ BM)/BCP/AI	280	0.58	8.36	69.35	3.36

TABLE 2. Device Performance Parameters for Best Performing Device Types A, B, and C (A = ITO/(PTB7/PC₇₀BM)/BCP/AI, B = ITO/PEDOT:PSS/(PTB7/PC₇₀BM)/BCP/AI and C = ITO/(rr-P3HT/s-SWNT)/(PTB7/PC₇₀BM)/BCP/AI under AM 1.5G, 1 sun illumination)

device type	V _{oc} (V)	J _{sc} (mA cm ⁻²)	FF (%)	PCE (%)
A = ITO/(PTB7/PC ₇₀ BM)/BCP/AI	0.66	15.50	55.04	5.63
B = ITO/PEDOT:PSS/(PTB7/PC ₇₀ BM)/BCP/AI	0.68	15.41	69.96	7.33
C = ITO/(rr-P3HT/s-SWNT)/(PTB7/PC ₇₀ BM)/BCP/AI	0.68	15.46	72.58	7.63

to act as an efficient HTL is the hole doping of s-SWNTs by rr-P3HT that increases the ionization potential of the nanotubes to 4.9 eV, which favorably aligns with the HOMO level of the rr-P3HT (5.2 eV) (Figure 4E) in the active layer. Furthermore, analysis of the UV-vis spectra given in Figure 1D clearly indicates the disappearance of the absorption edge at 460 nm in the nanohybrid spectrum corresponding to free rr-P3HT present in the medium. Therefore, considering the absence of free rr-P3HT within the nanohybrids, it is important to note that the enhancement of the PCE is solely due to the efficient hole carrier ability of the nanohybrids and not due to any form of free rr-P3HT present in the nanohybrid solution used to prepare the film.

Considering the high efficiency of the prepared nanohybrids as a hole extraction layer, a series of OPV devices were fabricated using the low band gap PTB7 (HOMO \sim 5.1, LUMO \sim 3.3) polymer as the donor material in the active layer. An optimized reference device without any HTL for comparison and an optimized device employing PEDOT:PSS was fabricated to study the potential of nanohybrids as compared to the widely used HTL standard.

Evaluation of the performance of self-ordered nanohybrid grids as a HTL was carried out based on three different multilayer device types, A, B, and C (Table 2), with an active layer comprising PTB7 and PC₇₀BM. While device A did not incorporate a HTL, device B consisted of a 40 nm thick PEDOT:PSS layer and device C contained a 1–3 nm thin network of nanohybrids as the HTL (Figure 4A).

The current density–voltage (J–V) characteristics of best performing devices A, B, and C under AM 1.5G illumination with an irradiation intensity of 100 mW cm⁻² are depicted in Figure 5A. Devices of type C, incorporating nanohybrid hole transport layers, were fabricated in the range of 100–180 nm active layer thicknesses,

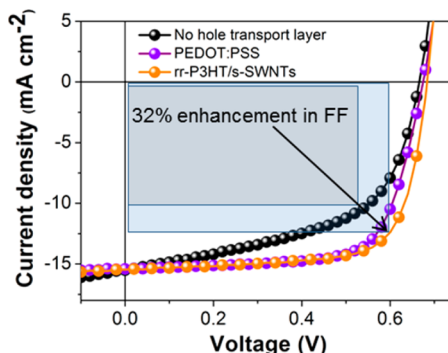


Figure 5. J–V characteristics of devices A, B, and C and a comparison of CNT incorporated OPVs. J–V characteristics of devices A (black line), B (purple line), and C (orange line) under AM 1.5G illumination with an irradiation intensity of 100 mW cm⁻². The same device architecture as in Figure 4 has been used here, and PTB7 is used in the active layer as the donor material. The plot displays the significant enhancement in the FF when a HTL layer is incorporated into the device architecture.

whereas the maximum efficiency of 7.6% was recorded at an active layer thickness of \sim 170 nm. Four devices of the same type were fabricated with an identical active layer thickness, and the PCE was in the range of 7.2–7.6%.

The potential of the nanohybrids to act as a HTL is proven by the significant improvement of 36% in the PCE of device type C compared to device type A, leading to a PCE of 7.6%, which is the highest reported for a carbon nanotube incorporated OPV to date. It is clearly noted that the enhanced PCE of device type C is governed by the enhanced FF of 73% compared to 55% of device type A.

It is evident that the nanohybrids are a potential candidate for replacing most HTLs, including the widely used PEDOT:PSS, considering the solar cell performances of the two devices B (PCE \sim 7.3%) and C (PCE \sim 7.6%). Four of the best performing type B devices were also fabricated, and the PCE was in the range of 7.1–7.3%. These were examined over different dates with all data showing consistent improvements to performance with the nanohybrid HTL.

For completion, the hole mobility (μ) of the fabricated devices was measured using nanohybrids and PEDOT:PSS as the HTL using space charge limited current (SCLC) analysis method (see Supporting Information). Both devices were identical in terms of materials employed and the layer thicknesses, the only difference being the HTL. The calculated μ of such nanohybrid HTL incorporated devices was 1.21×10^{-4} cm² V⁻¹ s⁻¹,

whereas the μ of PEDOT:PSS incorporated devices was $1.11 \times 10^{-4} \text{ cm}^2 \text{ V}^{-1} \text{ s}^{-1}$. Since, under identical conditions, the hole mobilities of both devices are comparable, it is reasonable to conclude that the hole mobility of nanohybrids is almost similar to the hole mobility of PEDOT:PSS. The better solar cell performance, higher light transmission through the HTL, and the lack of degradation of ITO due to the inert nature of nanohybrids makes the novel nanohybrid material a desirable candidate for hole extraction in OPVs and hole injection in OLEDs.

CONCLUSIONS

Preferential hole transport has been observed for the first time in a conjugated polymer-wrapped carbon nanotube network through spectroscopic analysis (XPS and Raman spectroscopy) and electrical measurements

(photoresponse of a hole only photovoltaic device and field effect transistor measurements). The hole transportation is facilitated by the downshifting of the nanotube ionization potential due to its hole doping by the surrounding polymer sheath.

The PCE of 7.6% for the nanohybrid photovoltaic device is the highest efficiency reported for BHJ OPV devices employing any type of carbon nanotubes to date. Our device is one of the most efficient organic solar cells over 50 mm^2 , where the majority of the reported best in class OPVs consist of device areas $<20 \text{ mm}^2$.^{45,46} These results will help in the design of future large area CNT hybrid OPVs and optoelectronic devices, considering the efficient charge extraction, low cost, low material consumption, high transparency, and the chemical inertness of the nanohybrid networks proposed.

METHODS

rr-P3HT Wrapping of s-SWNTs. A mass of 0.6 mg of rr-P3HT (Rieke Metals Inc., weight average molecular weight, $M_w = 50\,000 \text{ g mol}^{-1}$ and regioregularity = 95%) was added to 1.00 mL of chlorobenzene such that the concentration of rr-P3HT was 0.60 mg mL^{-1} and sonicated for 60 min. A mass of 0.50 mg of s-SWNTs (Nanointegris IsoNanotubes-s (90% semiconducting)) was added to the solution (0.5 mg mL^{-1}) and was ultrasonically treated at a frequency of 32–38 kHz for further 60 min. A volume of 1.00 mL of toluene was added to the solution mixture, sonicated for 15 min, and centrifuged for 8 min at 16000g in order to remove the excess rr-P3HT in the medium. The precipitate was collected, while the supernatant (dark yellow) was discarded. The above sonication and centrifugation procedure was performed twice more, and the precipitate was collected while the supernatant (pale yellow) was discarded. The precipitate obtained was dissolved in 1.0 mL of 1,2-dichlorobenzene by ultrasonication for 60 min such that the final concentration of rr-P3HT/s-SWNTs is $\sim 0.5 \text{ mg mL}^{-1}$.

Fabrication and Performance Measurement of OPV Devices. **rr-P3HT/PC₇₀BM Devices.** A mass of 20.00 mg each of rr-P3HT and PC₇₀BM (99% pure; Solenne) was added to 1.0 mL of 1,2-dichlorobenzene, and the solution was stirred overnight after which filtering of the solution was carried out using a $0.2 \mu\text{m}$ filter. **Device A:** ITO-coated glass which had been cleaned in an ultrasonic bath using acetone and methanol and subjected to an oxygen plasma treatment for 5 min was used to spin-coat the filtered rr-P3HT/PC₇₀BM active layer. A two-step spin-coating process was utilized for the spin-coating of the active layer; first step at 750 rpm for 40 s and second step at 1500 rpm for 1 s, which was found to yield optimal active layer thickness. **Device B:** A diluted solution ($\sim 0.02 \text{ mg mL}^{-1}$) of the original rr-P3HT/s-SWNT solution (0.5 mg mL^{-1}) was spin-coated on cleaned ITO-coated glass (same cleaning procedure as above) at a speed of 1500 rpm for 1 min and was annealed at a temperature of 120 °C for 10 min allowing the solvent to evaporate. The active layer consisting of rr-P3HT/PC₇₀BM was spin-coated on top of the rr-P3HT/s-SWNT film in a two-step process; first step at 500 rpm for 40 s and second step at 1500 rpm for 1 s.

The spin-coated devices were allowed to dry slowly in closed Petri dishes (60 mm diameter, 15 mm height) at room temperature, and the films were then annealed at 120 °C for 10 min. The hole-blocking layer, bathocuproine (BCP) (2 nm), and Al (70 nm) electrode (cathode) were then thermally evaporated under vacuum of $<3 \times 10^{-6} \text{ mbar}$, yielding a device with an area of $\sim 0.7 \text{ cm}^2$. All of the steps involved in device fabrication were carried out in a nitrogen-filled MBRAUN glovebox. Current density–voltage (J – V) measurements were performed using a Keithley 2400 exposing the devices to simulated AM 1.5G light (obtained from Abet Technologies-10500 solar simulator calibrated to an intensity of 1000 W m^{-2} with a Newport reference solar cell) at room temperature.

performed using a Keithley 2400 exposing the devices to stimulated AM 1.5G light (obtained from 300 W Xe Arc lamp ORIEL simulator calibrated to an intensity of 1000 W m^{-2} with a Newport reference solar cell) at room temperature.

PTB7/PC₇₀BM Devices. A mass of 10.00 mg of PTB7 (1-material Chemscitech Inc.) and 15.00 mg of PC₇₀BM (99% pure; Solenne) were added to 1.0 mL of chlorobenzene/1,8-diiodooctane (97:3 vol %), and the solution was stirred overnight at 70 °C, after which filtering of the solution was carried out using a $0.2 \mu\text{m}$ filter. **Device Type A:** ITO-coated glass was precleaned as described above. Spin-coating of the PTB7/PC₇₀BM active layer was carried out at 800 rpm for 2 min. **Device Type B:** A solution of PEDOT:PSS was spin-coated on cleaned ITO-coated glass (same cleaning procedure as above) at a speed of 5000 rpm for 40 s to obtain a thickness of 40 nm and was annealed at a temperature of 155 °C for 10 min. The active layer consisting of PTB7/PC₇₀BM was spin-coated at 1000 rpm for 2 min on top of the PEDOT:PSS film. **Device Type C:** A diluted solution ($\sim 0.02 \text{ mg mL}^{-1}$) of the original rr-P3HT/s-SWNT solution (0.5 mg mL^{-1}) was spin-coated on cleaned ITO-coated glass (as given above) at a speed of 1500 rpm for 1 min and was annealed at a temperature of 120 °C for 10 min allowing the solvent to evaporate. The active layer consisting of PTB7/PC₇₀BM was spin-coated at 600 rpm for 2 min on top of the rr-P3HT/s-SWNT film where the active layer thickness is 170 nm.

All devices were slow dried at room temperature. The hole-blocking layer, bathocuproine (BCP) (4 nm), and Al (80 nm) electrode (cathode) were then thermally evaporated under vacuum of $<3 \times 10^{-6} \text{ mbar}$, yielding a device with an area of 70 mm^2 . All of the steps involved in device fabrication were carried out in a nitrogen-filled MBRAUN glovebox. Current density–voltage (J – V) measurements were performed using a Keithley 2400 exposing the devices to simulated AM 1.5G light (obtained from Abet Technologies-10500 solar simulator calibrated to an intensity of 1000 W m^{-2} with a Newport reference solar cell) at room temperature.

“Hole Only” Device Fabrication and Measurement. Fabrication of devices was carried out on precleaned ITO-coated glass substrates as described above. The nanohybrid layers in 1,2-dichlorobenzene (0.01 mg mL^{-1}) were spin-coated onto the cleaned substrates inside an MBRAUN glovebox. Upon drying the substrate at $\sim 110 \text{ °C}$ for 10 min inside the glovebox, the active layer consisting of rr-P3HT (50 nm) was spin-coated onto the substrate at 750 rpm. Subsequently, 2 nm bathocuproine (electron-blocking layer) and 70 nm Al were thermally evaporated. Photovoltaic device measurements were carried out in air using an AM 1.5G solar simulator calibrated using a Si reference cell.

Field Effect Device Fabrication. Field effect devices with interdigitated electrode architectures (channel width of 2000 μm and channel length of 10 μm) were fabricated on 230 nm SiO₂ on n-type Si using standard photolithographic techniques. Spin-coating of the 0.02 mg mL⁻¹ nanohybrids was carried out inside an MBRAUN glovebox. Upon spin-coating, all devices were annealed at 110 °C for 10 min. Electrical characterization was carried out inside the glovebox using a Keithley 4200 SCS system using the Si substrate as a global back gate.

Film Thickness Measurements. The thickness measurements of the devices were carried out using an Alpha-step 200 profilometer.

UV–Vis–NIR Absorption Spectra. 1,2-Dichlorobenzene was used as the solvent to obtain solution phase absorption spectra of pristine rr-P3HT and nanohybrids. Pristine s-SWNTs were dispersed in deionized water using Triton X-100 as the surfactant. All measurements were carried out using a Varian Cary 5000 UV–vis spectrophotometer.

Optical Transmission Spectra. Films of rr-P3HT/s-SWNTs spin-coated on ITO substrates at 1500 rpm for 1 min and annealed at a temperature of 120 °C for 10 min was used to obtain the optical transmission through the nanohybrids. Measurements were carried out using a Varian Cary 5000 UV–vis spectrophotometer.

Raman Spectroscopic Analysis. Films of rr-P3HT/s-SWNTs spin-coated on ITO substrates and a buckypaper of s-SWNTs (as received) were used to obtain Raman spectra. The measurements were carried out using a Renishaw micro-Raman system with an Ar⁺ laser operating at a wavelength of 514.5 nm.

AFM Imaging of Nanohybrids. rr-P3HT/s-SWNT nanohybrids were spin-coated on ITO substrates to obtain AFM images, and the images were taken using a Veeco dimension 3000 instrument.

XPS Measurements. X-ray photoelectron measurements were conducted at the synchrotron beamline UE 52 PGM, Bessy II, Universität Würzburg, using a hemispherical SCIENTA SES 200 photoelectron energy analyzer. The base pressure in the setup was maintained below 10⁻¹⁰ mbar. Core level spectra of s-SWNTs and rr-P3HT/s-SWNTs were obtained using photon energies of 1250 and 400 eV, and valence level spectra were taken using a photon energy of 125 eV.

Conflict of Interest: The authors declare no competing financial interest.

Acknowledgment. This project is funded by E.ON AG as part of the E.ON International Research Initiative. G.D. acknowledges support from the Overseas Research Scholarship/University Research Scholarship—University of Surrey. K.J. acknowledges support from the EPSRC (Grant Number EP/F052901/1). M.P. acknowledges support from South East Physics Network (SEPNET). H.S. acknowledges support from the Leverhulme Trust.

Supporting Information Available: A magnified AFM image of the nanohybrids, the response of the “hole only” nanohybrid incorporated device under dark and illuminated conditions, method of fabrication of hole only devices and hole mobility calculations. This material is available free of charge via the Internet at <http://pubs.acs.org>.

REFERENCES AND NOTES

- Ahn, J.-H.; Kim, H.-S.; Lee, K. J.; Jeon, S.; Kang, S. J.; Sun, Y.; Nuzzo, R. G.; Rogers, J. A. Heterogeneous Three-Dimensional Electronics by Use of Printed Semiconductor Nanomaterials. *Science* **2006**, *314*, 1754–1757.
- Adikaari, A. A. D. T.; Dissanayake, D. M. N. M.; Silva, S. R. P. Hybrid Organic–Inorganic Solar Cells: Recent Developments and Outlook. *IEEE J. Sel. Top. Quantum Electron.* **2010**, *16*, 1595–1606.
- Lee, H. W.; Yoon, Y.; Park, S.; Oh, J. H.; Hong, S.; Liyanage, L. S.; Wang, H.; Morishita, S.; Patil, N.; Park, Y. J.; et al. Selective Dispersion of High Purity Semiconducting Single-Walled Carbon Nanotubes with Regioregular Poly-(3-alkylthiophene)s. *Nat. Commun.* **2011**, *2*, 541.
- Sawy, Z. S.; Davenport, M. Biosensors: Making Nanopores from Nanotubes. *Nat. Nanotechnol.* **2010**, *5*, 174–175.
- Nismy, N. A.; Adikaari, A. A. D. T.; Silva, S. R. P. Functionalized Multiwall Carbon Nanotubes Incorporated Polymer/Fullerene Hybrid Photovoltaics. *Appl. Phys. Lett.* **2010**, *97*, 033105–033103.
- Nish, A.; Hwang, J.-Y.; Doig, J.; Nicholas, R. J. Highly Selective Dispersion of Single-Walled Carbon Nanotubes Using Aromatic Polymers. *Nat. Nanotechnol.* **2007**, *2*, 640–646.
- Ren, S.; Bernardi, M.; Lunt, R. R.; Bulovic, V.; Grossman, J. C.; Gradečak, S. Toward Efficient Carbon Nanotube/P3HT Solar Cells: Active Layer Morphology, Electrical, and Optical Properties. *Nano Lett.* **2011**, *11*, 5316–5321.
- Bindl, D. J.; Wu, M.-Y.; Prehn, F. C.; Arnold, M. S. Efficiently Harvesting Excitons from Electronic Type-Controlled Semiconducting Carbon Nanotube Films. *Nano Lett.* **2010**, *11*, 455–460.
- Schuetzfort, T.; Nish, A.; Nicholas, R. J. Observation of a Type II Heterojunction in a Highly Ordered Polymer–Carbon Nanotube Nanohybrid Structure. *Nano Lett.* **2009**, *9*, 3871–3876.
- Bernardi, M.; Giulianini, M.; Grossman, J. C. Self-Assembly and Its Impact on Interfacial Charge Transfer in Carbon Nanotube/P3HT Solar Cells. *ACS Nano* **2010**, *4*, 6599–6606.
- Dissanayake, N. M.; Zhong, Z. H. Unexpected Hole Transfer Leads to High Efficiency Single-Walled Carbon Nanotube Hybrid Photovoltaic. *Nano Lett.* **2011**, *11*, 286–290.
- Han, J.-H.; Paulus, G. L. C.; Maruyama, R.; Heller, D. A.; Kim, W.-J.; Barone, P. W.; Lee, C. Y.; Choi, J. H.; Ham, M.-H.; Song, C.; et al. Exciton Antennas and Concentrators from Core–Shell and Corrugated Carbon Nanotube Filaments of Homogeneous Composition. *Nat. Mater.* **2010**, *9*, 833–839.
- Henley, S. J.; Hatton, R. A.; Chen, G. Y.; Gao, C.; Zeng, H.; Kroto, H. W.; Silva, S. R. P. Enhancement of Polymer Luminescence by Excitation-Energy Transfer from Multi-Walled Carbon Nanotubes. *Small* **2007**, *3*, 1927–1933.
- Nismy, N. A.; Jayawardena, K. D. G. I.; Adikaari, A. A. D. T.; Silva, S. R. P. Photoluminescence Quenching in Carbon Nanotube–Polymer/Fullerene Films: Carbon Nanotubes as Exciton Dissociation Centres in Organic Photovoltaics. *Adv. Mater.* **2011**, *23*, 3796–3800.
- Miller, A. J.; Hatton, R. A.; Silva, S. R. P. Interpenetrating Multiwall Carbon Nanotube Electrodes for Organic Solar Cells. *Appl. Phys. Lett.* **2006**, *89*, 133117.
- Sun, Y. M.; Gong, X. O.; Hsu, B. B.; Yip, H. L.; Jen, A. K. Y.; Heeger, A. J. Solution-Processed Cross-Linkable Hole Selective Layer for Polymer Solar Cells in the Inverted Structure. *Appl. Phys. Lett.* **2010**, *97*, 193310.
- Hatton, R. A.; Blanchard, N. P.; Stoljan, V.; Miller, A. J.; Silva, S. R. P. Nanostructured Copper Phthalocyanine-Sensitized Multiwall Carbon Nanotube Films. *Langmuir* **2007**, *23*, 6424–6430.
- Chaudhary, S.; Lu, H.; Müller, A. M.; Bardeen, C. J.; Ozkan, M. Hierarchical Placement and Associated Optoelectronic Impact of Carbon Nanotubes in Polymer–Fullerene Solar Cells. *Nano Lett.* **2007**, *7*, 1973–1979.
- Schuetzfort, T.; Snaith, H. J.; Nish, A.; Nicholas, R. J. Synthesis and Spectroscopic Characterization of Solution Processable Highly Ordered Polythiophene–Carbon Nanotube Nanohybrid Structures. *Nanotechnology* **2010**, *21*, 025201.
- Dang, X.; Yi, H.; Ham, M.-H.; Qi, J.; Yun, D. S.; Ladewski, R.; Strano, M. S.; Hammond, P. T.; Belcher, A. M. Virus-Templated Self-Assembled Single-Walled Carbon Nanotubes for Highly Efficient Electron Collection in Photovoltaic Devices. *Nat. Nanotechnol.* **2011**, *6*, 377–384.
- Giulianini, M.; Waclawik, E. R.; Bell, J. M.; Scarselli, M.; Castrucci, P.; De Crescenzi, M.; Motta, N. Microscopic and Spectroscopic Investigation of Poly(3-hexylthiophene) Interaction with Carbon Nanotubes. *Polymers* **2011**, *3*, 1433–1446.
- Giulianini, M.; Waclawik, E. R.; Bell, J. M.; Scarselli, M.; Castrucci, P.; De Crescenzi, M.; Motta, N. Poly(3-hexylthiophene) Coil-Wrapped Single Wall Carbon Nanotube

Investigated by Scanning Tunneling Spectroscopy. *Appl. Phys. Lett.* **2009**, *95*, 143116–143113.

23. Goh, R. G. S.; Motta, N.; Bell, J. M.; Waclawik, E. R. Effects of Substrate Curvature on the Adsorption of Poly(3-hexylthiophene) on Single-Walled Carbon Nanotubes. *Appl. Phys. Lett.* **2006**, *88*, 053101–053103.
24. Giuliani, M. Regioregular Poly(3-hexylthiophene) Helical Self-Organization on Carbon Nanotubes. *Appl. Phys. Lett.* **2009**, *95*, 013304.
25. Kuila, B. K.; Park, K.; Dai, L. Soluble P3HT-Grafted Carbon Nanotubes: Synthesis and Photovoltaic Application. *Macromolecules* **2010**, *43*, 6699–6705.
26. Salleo, A.; Kline, R. J.; DeLongchamp, D. M.; Chabiny, M. L. Microstructural Characterization and Charge Transport in Thin Films of Conjugated Polymers. *Adv. Mater.* **2010**, *22*, 3812–3838.
27. Danner, P. The Chemical and Electronic Structure of the Interface between Aluminum and Polythiophene Semiconductors. *J. Chem. Phys.* **1993**, *99*, 664.
28. Feng, D. Q.; Caruso, A. N.; Schulz, D. L.; Losovyj, Y. B.; Dowben, P. A. Photohole Screening Effects in Polythiophenes with Pendant Groups. *J. Phys. Chem. B* **2005**, *109*, 16382–16389.
29. Wei, H.; Scudiero, L.; Eilers, H. Infrared and Photoelectron Spectroscopy Study of Vapor Phase Deposited Poly(3-hexylthiophene). *Appl. Surf. Sci.* **2009**, *255*, 8593–8597.
30. Kanai, K.; Miyazaki, T.; Suzuki, H.; Inaba, M.; Ouchi, Y.; Seki, K. Effect of Annealing on the Electronic Structure of Poly(3-hexylthiophene) Thin Film. *Phys. Chem. Chem. Phys.* **2010**, *12*, 273–282.
31. Salaneck, W. Thermochromism in Poly(3-hexylthiophene) in the Solid State: A Spectroscopic Study of Temperature Dependent Conformational Defects. *J. Chem. Phys.* **1988**, *89*, 4613.
32. Shrotriya, V.; Ouyang, J.; Tseng, R. J.; Li, G.; Yang, Y. Absorption Spectra Modification in Poly(3-hexylthiophene): Methanofullerene Blend Thin Films. *Chem. Phys. Lett.* **2005**, *411*, 138–143.
33. Rao, A. M.; Eklund, P. C.; Bandow, S.; Thess, A.; Smalley, R. E. Evidence for Charge Transfer in Doped Carbon Nanotube Bundles from Raman Scattering. *Nature* **1997**, *388*, 257–259.
34. Asadi, K.; De Leeuw, D. M.; De Boer, B.; Blom, P. W. M. Organic Non-volatile Memories from Ferroelectric Phase-Separated Blends. *Nat. Mater.* **2008**, *7*, 547–550.
35. Appenzeller, J.; Yu-Ming, L.; Knoch, J.; Zhihong, C.; Avouris, P. Comparing Carbon Nanotube Transistors—The Ideal Choice: A Novel Tunneling Device Design. *IEEE Trans. Electron Devices* **2005**, *52*, 2568–2576.
36. Dai, H. J.; Javey, A.; Guo, J.; Wang, Q.; Lundstrom, M. Ballistic Carbon Nanotube Field-Effect Transistors. *Nature* **2003**, *424*, 654–657.
37. Yahya, I.; Stolojan, V.; Clowes, S.; Mustaza, S. M.; Silva, S. R. P. *Carbon Nanotube Field Effect Transistor Measurements in Vacuum*, IEEE International Conference on Semiconductor Electronics (ICSE), Melaka, Malaysia, 28–30 June, **2010**; pp 224–228.
38. Bao, Z. N.; LeMieux, M. C.; Roberts, M.; Barman, S.; Jin, Y. W.; Kim, J. M. Self-Sorted, Aligned Nanotube Networks for Thin-Film Transistors. *Science* **2008**, *321*, 101–104.
39. Choulis, S. A.; Kim, Y.; Nelson, J.; Bradley, D. D. C.; Giles, M.; Shkunov, M.; McCulloch, I. High Ambipolar and Balanced Carrier Mobility in Regioregular Poly(3-hexylthiophene). *Appl. Phys. Lett.* **2004**, *85*, 3890–3892.
40. Brabec, C. J.; Dyakonov, V. Photoinduced Charge Transfer in Bulk Heterojunction Composites. In *Organic Photovoltaics: Concepts And Realization*; Brabec, C. J., Dyakonov, V., Parisi, J., Sariciftci, N. S., Eds.; Springer: New York, 2003; pp 92–96.
41. Scharber, M. C.; Mühlbacher, D.; Koppe, M.; Denk, P.; Waldauf, C.; Heeger, A. J.; Brabec, C. J. Design Rules for Donors in Bulk-Heterojunction Solar Cells—Towards 10% Energy-Conversion Efficiency. *Adv. Mater.* **2006**, *18*, 789–794.
42. Stranks, S. D.; Weissfennig, C.; Parkinson, P.; Johnston, M. B.; Herz, L. M.; Nicholas, R. J. Ultrafast Charge Separation at a Polymer–Single-Walled Carbon Nanotube Molecular Junction. *Nano Lett.* **2011**, *11*, 66–72.
43. Wu, M. C.; Lin, Y. Y.; Chen, S.; Liao, H. C.; Wu, Y. J.; Chen, C. W.; Chen, Y. F.; Su, W. F. Enhancing Light Absorption and Carrier Transport of P3HT by Doping Multi-Wall Carbon Nanotubes. *Chem. Phys. Lett.* **2009**, *468*, 64–68.
44. Beek, W. J. E.; Janssen, R. A. J. Hybrid Polymer-Inorganic Photovoltaic Cells. In *Hybrid Nanocomposites For Nanotechnology: Electronic, Optical, Magnetic and Bio/Medical Applications*; Merhari, L., Ed.; Springer: New York, 2009; pp 354–358.
45. Liang, Y.; Xu, Z.; Xia, J.; Tsai, S.-T.; Wu, Y.; Li, G.; Ray, C.; Yu, L. For the Bright Future—Bulk Heterojunction Polymer Solar Cells with Power Conversion Efficiency of 7.4%. *Adv. Mater.* **2010**, *22*, E135–E138.
46. Sun, Y.; Welch, G. C.; Leong, W. L.; Takacs, C. J.; Bazan, G. C.; Heeger, A. J. Solution-Processed Small-Molecule Solar Cells with 6.7% Efficiency. *Nat. Mater.* **2012**, *11*, 44–48.